Extended Limits on Neutral Strongly Interacting Massive Particles and Nuclearites from NaI(Tl) Scintillators

R. Bernabei, P. Belli, R. Cerulli, and F. Montecchia

Dipartimento di Fisica, Universita' di Roma "Tor Vergata" and INFN, Sezione di Roma2, I-00133 Rome, Italy

M. Amato, G. Ignesti, A. Incicchitti, and D. Prosperi

Dipartimento di Fisica, Universita' di Roma "La Sapienza" and INFN, Sezione di Roma, I-00185 Rome, Italy

C. J. Dai, H. L. He, H. H. Kuang, J. M. Ma, G. X. Sun, and Z. Ye

IHEP, Chinese Academy, P.O. Box 918/3, Beijing 100039, China
(Received 8 June 1999)

Neutral strongly interacting massive particles (SIMPs) were searched for at the Gran Sasso National Laboratory by using two "planes" of detectors in the $\simeq 100$ kg highly radiopure NaI(Tl) DAMA setup. SIMP exclusion plots and model-independent limits on neutral nuclearites have been significantly improved.

In this paper we present results on a further search for neutral strongly interacting massive particles (SIMPs), that is, neutral particles with masses (M_S) between few GeV and the grand unified theory scale and cross sections on protons (σ_p) up to $\simeq 10^{-22}$ cm^2, embedded in the galactic halo (therefore, with $\beta \simeq 10^{-3}$). Candidates of this kind could be formed, e.g., by the "neutralization" of exotic particles (with electromagnetic and/or nuclear charge) with ordinary matter during primordial nucleosynthesis; therefore, they have also been investigated by searching for anomalous heavy nuclei in terrestrial samples [1]. Moreover, it has been suggested that SIMPs could be the sources of ultrahigh-energy cosmic rays [2] and that in some models of supersymmetry breaking they could appear as, e.g., gluino lightest supersymmetric particles [3]. In spite of their large cross sections, SIMPs [4,5] should have a relatively low interaction rate due to their low density in the galactic halo. Some discussion on possible abundance and cosmological interest can be found in Ref. [6]. A detailed analysis of the available data was performed in Ref. [7] Starkman *et al.*; further limits on σ_p versus M_S have then been achieved in Refs. [8–10].

The present result has been obtained by searching for delayed coincidences between two "planes" of detectors in the $\simeq 100$ kg NaI(Tl) dark matter (DAMA) experimental setup [11–17] during 350.05 days. The setup is placed deep underground in the Gran Sasso National Laboratory of INFN [18] at 42°27' north latitude, and it is shielded from cosmic rays by a rock depth of about 3400 mwe (meter of water equivalent). The overlaying rock degrades the SIMPs energy and reduces the setup sensitivity to large cross sections, but the low background technique and the μ flux reduction allow the SIMPs search to be extended to lower fluxes and higher masses.

In the following we also utilize the data previously collected at Gran Sasso with another of our setups, the one named F in Ref. [10], while we do not consider here the

data we obtained with the test setups (P_1, P_2) described in Ref. [9], because of both the marginal statistics and the higher energy threshold.

Finally, the experimental data are also used to set improved model-independent upper limits on the flux of neutral nuclearites.

Experimental procedure and results.—Following the suggestion of Ref. [4] and according to Refs. [9,10], two parallel planes—each one made up of three 9.70 kg (10.2-cm large, 10.2-cm thick, and 25.4-cm long) low radioactive NaI(Tl) detectors—have been used to search for delayed coincidences from SIMP elastic scattering on sodium and/or iodine nuclei during 350.05 days; the measured quantities are the recoil energies. The two planes–23.2 cm center-to-center distance—are separated by another identical "plane" not considered in the trigger (see Fig. 1). They are part of the $\simeq 100$ kg highly radiopure NaI(Tl) DAMA setup described in detail in Ref. [11]. Each detector has two 10-cm-long tetrasil-B light guides directly coupled to the opposite sides of the bare crystal; two photomultipliers EMI9265-B53/FL work in coincidence at the single photoelectron threshold. A low radioactive Cu box—inside a multicomponent low radioactive shield—houses the detectors, maintaining them in high purity nitrogen atmosphere [11]. The knowledge of the energy scale is ensured by periodic calibrations and by monitoring the position and resolution of the 46.5 keV ^{210}Pb peak in the production data [11]. (This peak is present at a level of a few cpd/kg in the measured energy distributions, mainly because of a surface contamination by environmental radon which occurred during the first period of the detectors' underground storage.)

Delayed coincidences corresponding to both "downward" (d) and "upward" (u) patterns are acquired, that is, coincidences in which a scintillation pulse in one detector of a plane is followed—within 350–3000 ns—by
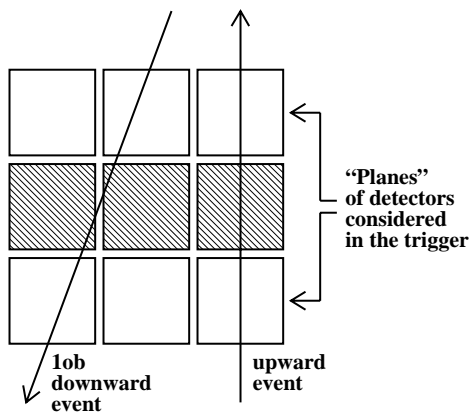
FIG. 1. Schematic front view of the detectors (see text).

another scintillation pulse in one detector of the other plane. The pulse profiles are recorded by a Lecroy transient digitizer model 2262 and the fired crystals are identified. The present data set corresponds to a total exposure of 1.1×10^6 cm^2 sr day.

According to the previous analysis of Ref. [10] we have considered here two energy regions: a 4–60 keV electron equivalent for mainly single scattering events and above 60 keV electron equivalent for multiple scatterings inside the crystals, giving pulses with many bumps and long-time structure. Similar pulses are expected when the cross section on the target nucleus is much larger than $(n \cdot d)^{-1}$, with n the number density of the target nuclei (1.47×10^{22} ^{23}Na or ^{127}I nuclei per cm^3) and d the crossed crystal's depth ($\simeq 10.2$ cm). A summary of the observed $d + u$ delayed coincidences—in the mainly single scattering region—is shown in Table I. The event in the second row of Table I is shown—as an example— in Fig. 2.

The expected random coincidences in the 4–60 keV energy region during 350.05 days of running time (T) are: $R_1 \times R_2 \times \Delta t \times T = 0.2$, where R_1 and R_2 are the single counting rates measured by the two planes of detectors in the considered energy region; Δt is the coincidence time window (2.65 μs) used here. Moreover, according to Ref. [9], significant contributions from correlated processes induced by environmental neutrons [19] can be excluded. In particular, with regard to the possible thermal neutron capture on ^{127}I nuclei, exciting ^{128m}I long-lived isomeric states [20], a contribution <0.1 counts [90% confidence level (C.L.)] to the $d + u$ patterns during 350.05 days has been estimated by Monte Carlo calculations properly considering the measured upper limit on ^{128m}I decays in our detectors [11].

In summary, with regard to the mainly single scattering energy region, the upper limit on the number of $d + u$ delayed coincidences has been derived by considering a Poissonian distribution with background [21], having 0.2 delayed coincidences expected and two observed; the limit is <5.12 events at 90% C.L. Furthermore, no delayed coincidence with multibump/long-time structure

TABLE I. Summary of the measured delayed coincidences in the mainly single scattering region; 1ob indicates an oblique pattern in the two planes between first close detectors.

E_1 (keV)	E_2 (keV)	Δt (ns)	Direction	Pattern
18.3	45.9	1975	downward	1ob
13.4	53.4	362.5	downward	1ob

has been detected in the 350.05 days. Therefore, the upper limit on the number of events in the multiple scattering region—calculated with the same approach [21] for $d + u$ delayed coincidences—results in <2.3 events at 90% C.L., having never observed a multibump/long-time structure event.

As mentioned above, the results presented in the following include also the data we collected at Gran Sasso with our F setup (two planes of two 7.05 kg NaI(Tl) detectors each) and already considered in Ref. [10]. Zero delayed coincidences were observed in both energy regions, for a total exposure of 132 980 cm^2 sr day. The proper features (such as, e.g., geometry and used time window) have been taken into account.

Exclusion plots for neutral SIMPs.—To interpret data collected in underground experiments it is necessary to evaluate the effect of the matter crossed by the SIMPs. Therefore, we accounted for the chemical composition of the overlaying mountain [22] in the case of downward delayed coincidences and for the mean composition of the different regions inside the Earth (see Table I in Ref. [23]) in case of upward delayed coincidences, together with the different SIMP cross sections on the involved nuclei. As discussed in Ref. [10], the main effect of the material is the degrading of the SIMP velocity; this has been estimated by Monte Carlo calculations [22] and properly taken into account.
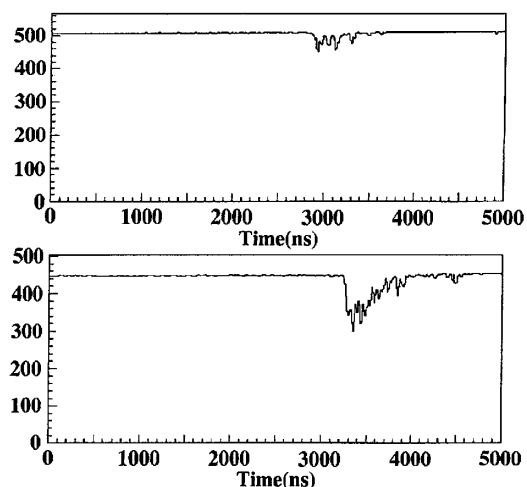

FIG. 2. The two scintillation pulses of the downward delayed coincidence described in the second row of Table I as recorded by a Lecroy transient digitizer model 2262. The vertical axis represents the pulse amplitude in arbitrary units.

With regard to the needed astrophysical assumptions, the SIMPs are considered here to be trapped in the gravitational field of the Galaxy with a quasi-Maxwellian velocity distribution having $v_{\text{rms}} = 270$ km/s (that is, of the order of the virial velocity of the galactic halo) and an escape cut-off velocity of 650 km/s. The solar system velocity in the galactic halo is 232 km/s so that the SIMP average velocity in the solar system frame (resulting from the convolution of the orbital and galactic velocities) is $\langle v \rangle = 331$ km/s. The local galactic halo density is assumed to be $\rho_S = 0.3$ GeV/cm^3.

Both interactions with sodium and iodine nuclei have been taken into account in our calculations. Therefore, the expected counting rates for both upward and downward delayed coincidences between the two planes of detectors in the mainly single scattering energy region are given by the sum of four terms (depending on the pairs of nuclei involved in the scattering processes) of the following form:

$$
\begin{aligned}
R_{d+u}^{A_1,A_2} &= \int \frac{dR_1}{d^3 v} P_2(\sigma_{A_2}, \hat{v}) d^3 v \\
&= \sigma_{A_1} \sigma_{A_2} \frac{\rho_S}{M_S} N_1 N_2 \left(\langle v \rangle \frac{\epsilon_\Omega \, \epsilon_{\text{tec}}^{A_1,A_2}}{S^{\text{eff}}} \right) f(\sigma_{A_1}, \sigma_{A_2}).
\end{aligned}
\tag{1}
$$

Here 1 and 2 identify the first and second hit planes, respectively; A_1 (A_2) identifies the nucleus (^{23}Na or ^{127}I) which is scattered in the first (second) hit plane; σ_{A_i} is the SIMP elastic cross section on the type of nucleus scattered in the ith plane and N_i is the corresponding number of nuclei in that plane. Moreover, S^{eff} is the effective surface of the setup; ϵ_Ω is the solid angle of the second hit plane as seen by the first one, normalized to 4π sterad; $\epsilon_{\text{tec}}^{A_1,A_2}$ represents the energy and time detection efficiency averaged over the flux of impinging particles and depends also on cross sections. The integral of Eq. (1) is performed over the velocities of the particles crossing both planes. The probability of an interaction in the ith hit plane along the d_i path identified by the SIMP velocity, $\hat{v}$, is $dR_i/d^3 v = (dn/d^3 v)(\rho_S/M_S) v [V_i/d_i(\hat{v})] P_i(\sigma_{A_i}, \hat{v})$ with $P_i(\sigma_{A_i}, \hat{v}) = 1 - e^{-[(N_i/V_i)\sigma_{A_i} d_i(\hat{v})]}$ and $(N_i/V_i)\sigma_{A_i}$ reciprocal of the mean-path free of the particle inside the ith plane of volume V_i. Finally, $f(\sigma_{A_1}, \sigma_{A_2}) = \langle P_1(\sigma_{A_1}, \hat{v}) \cdot P_2(\sigma_{A_2}, \hat{v}) \rangle / \langle [(N_1/V_1)\sigma_{A_1} d_1(\hat{v})][(N_2/V_2)\sigma_{A_2} d_2(\hat{v})] \rangle$.

In the multiple scattering case, when $\sigma_{A_i} \gg V_i/(N_i \langle d \rangle)$ ($\langle d \rangle$ being the mean path of the SIMPs inside the detectors), Eq. (1) can be written in the simpler form:

$$
R_{d+u} \simeq \frac{\rho_S}{M_S} \langle v \rangle S^{\text{eff}} \epsilon_\Omega \epsilon_{\text{tec}},
\tag{2}
$$

where ϵ_{tec} is the efficiency to detect SIMPs in the considered multiple scattering energy region and time window; it also depends on cross sections.

Moreover, according to Ref. [7], the SIMP-proton cross section has been considered to allow comparison with the results obtained by different experiments. It is related to σ_{A_i} by the following formulas: (a) spin-independent (SI) case, $\sigma_{A_i} = \sigma_p [m_{\text{red}}^2(A_i, M_S)]/[m_{\text{red}}^2(p, M_S)] A_i^2$, and (b) spin-dependent (SD) case, $\sigma_{A_i} = \sigma_p [m_{\text{red}}^2(A_i, M_S)]/[m_{\text{red}}^2(p, M_S)]$, having assumed in this latter case—according to Refs. [7,9,10]—the spin factors equal to unity. Here, $m_{\text{red}}(A, M_S)$ is the reduced mass between the A nucleus and the SIMP of mass M_S.

Specific calculations of the nuclear form factors are not available for SIMP interactions with ordinary matter; here, for simplicity, we follow the same assumption as in Refs. [9,10]. Moreover, the quenching factors we measured [12] for Na and I nuclei in NaI(Tl), $q_{\text{Na}} = 0.3$ and $q_{\text{I}} = 0.09$, are used to determine the energy scale for recoils.

Finally, the exclusion plots at 90% C.L. in the σ_p versus M_S plane for both SI and SD interactions have been determined by comparing the experimental upper limits on the $d + u$ delayed coincidences (achieved with present and F setups) with their expectations as a function of M_S and σ_p. The results are shown in Fig. 3.

The present analysis confirms and extends the previously excluded regions; in particular, the maximum reachable M_S is increased here up to $M_S \simeq 4 \times 10^{16}$ GeV.
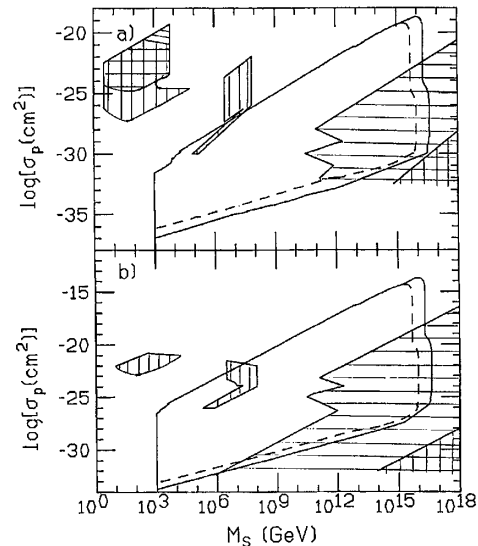

FIG. 3. The solid contours represent the obtained 90% C.L. exclusion plots in the plane SIMP cross section on proton versus SIMP mass: (a) SI interactions, (b) SD interactions; the excluded regions are inside the contours. The dashed lines account for the previous results of Refs. [8–10]. Moreover, for comparison, the regions allowed by the global analysis of Starkman et al. [7] for various cases are also shown: (i) presence of asymmetry in the terrestrial abundance of SIMPs and anti-SIMPs (vertically hatched regions); (ii) absence of SIMP–anti-SIMP asymmetry (horizontally hatched regions); (iii) unconstrained case (cross-hatched regions)—see Ref. [7] for details (note that only regions with $\sigma_p \geq 10^{-32}$ cm^2 were considered). As can be observed, two regions are largely explorable by experiments performed deep underground, while the third one ($\sigma_p \simeq 10^{-24}$ cm^2 and low M_S) can be investigated only by balloon or satellite experiments.
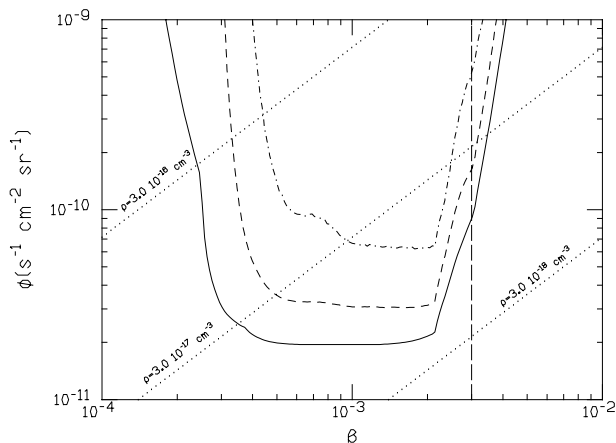
FIG. 4. Model-independent 90% C.L. limit contour on the flux of neutral nuclearites; the excluded region is inside. The solid line is the geometrical limit, which corresponds to $\sigma_p \gtrsim 10^{-28}$ cm^2 for SI interactions with $M_S > 10^6$ GeV and to $\sigma_p \gtrsim 10^{-24}$ cm^2 for SD interactions with $M_S > 10^5$ GeV (consider, e.g., the upper lines of the exclusion plots in Fig. 3 which account for the shield of the mountain). The slanted dotted lines indicate the neutral nuclearites' iso-number densities. Neutral nuclearite velocities, β, above the vertical long-dashed line correspond to particles with velocities large enough to escape from the gravitational field of the Galaxy. The dependence on σ_p is also shown for the SI case by the dashed line ($\sigma_p = 1.5 \times 10^{-30}$ cm^2) and by the dot-dashed line ($\sigma_p = 1.0 \times 10^{-30}$ cm^2).

Neutral nuclearites.—The results obtained in the multiple scattering region can also be used to calculate a model-independent upper limit on slow moving neutral nuclearites.

The nuclearites may constitute a new form of matter, which would contain roughly an equal number of up, down, and strange quarks; they have already been searched for by using several different techniques [10,24]. Here, considering that in the multiple scattering region the rate of neutral nuclearites depends only on geometrical factors (being the cross section large enough to always induce a total detected energy above 60 keV), the flux of nuclearites can be written as $\Phi = N_{\text{nucl}}/(S^{\text{eff}} \epsilon_\Omega \epsilon_{\text{tec}} T)$, where T is the running time and N_{nucl} is the number of events that can be ascribed to neutral nuclearites crossing the setup. Because no event has been detected in the multiple scattering region, we get $N_{\text{nucl}} < 2.3$ events at 90% C.L. Combining these results with the one achieved in Ref. [10] by the F setup and specializing here in the calculation of ϵ_{tec} to the case of $\beta \simeq 10^{-3}$ (virial velocity of the Galaxy), a model-independent upper limit at 90% C.L. can be obtained: $\Phi < 1.9 \times 10^{-11}$ s^{-1} cm^{-2} sr^{-1}. Relaxing the requirement on the β value, the model-independent 90% C.L. limit contour on the flux of neutral nuclearites as a function of β can be determined as shown in Fig. 4 (the poorer limits on Φ at $\beta \gtrsim 2 \times 10^{-3}$ and $\beta \lesssim 4 \times 10^{-4}$ are due to the decreasing of ϵ_{tec}). In the same figure the dependence of the limit contour on σ_p

is also shown for the SI case; in fact, when decreasing the cross section, the number of SIMP interactions in a single detector and the corresponding total detected energy decrease, lowering the detection efficiency in the given energy and time windows.

Conclusion.—The present analysis improves the excluded regions in the σ_p versus M_S plane with respect to previous searches [7–10], increasing the explored masses up to $M_S \simeq 4 \times 10^{16}$ GeV and allows one to obtain an improved model-independent upper limit on the flux of neutral nuclearites. In the "geometrical limit" the latter is $\Phi < 1.9 \times 10^{-11}$ s^{-1} cm^{-2} sr^{-1} at 90% C.L. ($\beta \simeq 10^{-3}$).

[1] J. Rich *et al.,* Phys. Lett. B **194**, 173 (1987); T. K. Hemmick *et al.,* Phys. Rev. D **41**, 2074 (1990).

[2] D. Chung, G. Farrar, and E. W. Kolb Phys. Rev. D **57**, 4606 (1998); C. Albuquerque, G. Farrar, and E. W. Kolb, Phys. Rev. D **59**, 015021 (1999); V. Berezinsky and M. Kalcheriess, Phys. Lett. B **422**, 163 (1998); V. Berezinsky and B. L. Ioffe, Sov. Phys. JETP **63**, 920 (1986).

[3] R. N. Mohapatra and S. Nandi, Phys. Rev. Lett. **79**, 181 (1997); S. Raby, Phys. Rev. D **56**, 2852 (1997).

[4] M. W. Goodman and E. Witten, Phys. Rev. D **31**, 3059 (1985).

[5] S. Dimopoulos *et al.,* Phys. Rev. D **41**, 2388 (1990); A. De Rujula, S. Glashow, and U. Sarid, Nucl. Phys. B **33**, 173 (1990).

[6] R. N. Mohapatra and S. Nussinov, Phys. Rev. D **57**, 1940 (1998); R. N. Mohapatra and V. L. Teplitz, Phys. Rev. Lett. **81**, 3079 (1998).

[7] G. D. Starkman *et al.,* Phys. Rev. D **41**, 3594 (1990).

[8] D. O. Caldwell, Nucl. Phys. (Proc. Suppl.) **28A**, 273 (1992).

[9] C. Bacci *et al.,* Astropart. Phys. **2**, 13 (1994).

[10] C. Bacci *et al.,* Astropart. Phys. **4**, 195 (1996).

[11] R. Bernabei *et al.,* Il Nuovo Cimento **112A**, 545 (1999).

[12] R. Bernabei *et al.,* Phys. Lett. B **389**, 757 (1996).

[13] R. Bernabei *et al.,* Phys. Lett. B **408**, 439 (1997).

[14] R. Bernabei *et al.,* Phys. Lett. B **424**, 195 (1998).

[15] R. Bernabei *et al.,* Phys. Lett. B **450**, 448 (1999).

[16] R. Bernabei *et al.,* Phys. Lett. B **460**, 235 (1999).

[17] P. Belli *et al.,* Phys. Rev. C **60**, 065501 (1999).

[18] E. Bellotti, Nucl. Instrum. Methods Phys. Res., Sect. A **264**, 1 (1988).

[19] P. Belli *et al.,* Il Nuovo Cimento **101A**, 959 (1989).

[20] A. Fubini *et al.,* Lett. Nuovo Cimento **3**, 785 (1970).

[21] K. Hikasa *et al.,* Phys. Rev. D **45**, III.40 (1992).

[22] H. Bilokon (private communication); W. Di Nicolantonio, thesis, Universita "La Sapienza," Roma, A.A., 1993/1994.

[23] J. I. Collar and F. T. Avignone III, Phys. Rev. D **47**, 5238 (1993).

[24] A. De Rújula and S. L. Glashow, Nature (London) **312**, 734 (1984); MACRO Collaboration, S. Ahlen *et al.,* Phys. Rev. Lett. **69**, 1860 (1992).